Microscopic Cross Section Calculations with NUCLEUS and HETC-3STEP

H.Takada, Y.Nakahara, T.Nishida
Japan Atomic Energy Research Institute

K.Ishibashi
Kyushu University

N.Yoshizawa
Mitsubishi Research Institute Inc.

Abstract

Benchmark calculations have been carried out for the double differential cross sections of (p,xp) and (p,xn) reactions at incident energies of 25 to 1500 MeV using the codes NUCLEUS and HETC-3STEP which are based on the intranuclear cascade evaporation model including the high energy fission. It has been found that NUCLEUS gives satisfactory agreements with the experimental data on the neutron double differential cross sections at intermediate energies of 25 to 1500 MeV. As the incident energy decreases, the code underestimates the backward nucleon emission spectra significantly. On the other hand, HETC-3STEP improves the defect of NUCLEUS by taking the preequilibrium process into account and makes it possible to predict the cross sections quite well even at several tens of MeV. The calculated results of HETC-3STEP agree with the experimental nuclide production cross sections within a factor of two.

1. Introduction

With the recent progress of accelerator technology, interests are growing for the application of accelerator to the engineering facilities such as spallation neutron sources and accelerator-based transmutation systems. From the view point of nuclear engineering, the accelerator-based transmutation system is of interest as one of options for the disposal of high level long-lived radioactive wastes. Some concepts have been proposed on the systems which consist of an intense proton accelerator with energy of 0.8 to 1.6 GeV and a subcritical core.[1-5] These concepts are based on the ideas[6] proposed in 1970s as systems for fertile to fissile material conversion. In these systems, protons are injected in a spallation target surrounded with a blanket region made of actinides and/or fission products. As the target, heavy metals i.e. tungsten or liquid lead-bismuth is considered to be favorable because of its efficient neutron yield per incident proton. For the component of blanket region, there are two options. One is the metal alloy fuel with sodium coolant for the transmutation with fast neutrons. The other is molten salt or aqueous fuel with heavy water coolant for the one with thermal neutrons.

Neutron yield and neutron energy spectra are important factors for the estimation of transmutation performance and radiation shielding of such systems. Hence, accurate nuclear data are required for a variety of nuclides over very wide energy range from eV to GeV. Because there are few nuclear data available above 20 MeV yet, requirements for an evaluated nuclear data file aiming at accelerator-based transmutation have been reported from OECD/NEA.[7] Moreover, a review[8] has been made on the calculation codes and the available experimental data for nuclear data evaluation in the intermediate energy region of 20 to 1600 MeV.

As for the neutronics calculation in the intermediate energy region, the simulation code based on an intranuclear cascade[9] evaporation[10] (INCE) model was developed and various supplements have been added so far. The authors have used NMTC/JAERI[11] for the neutronics calculation on a thick target. For the simulation on microscopic nuclear reactions, the code NUCLEUS[12] has been employed. This code is the nuclear reaction calculation part of NMTC/JAERI. In NUCLEUS, the spallation reaction is analyzed with the INCE model including the high energy fission process proposed by Nakahara[13]. Some studies[14,15] were made on the mass yield through the spallation reaction and the high energy fission reaction. It has been found that a large difference is seen in the calculated mass yield in comparison with a fission model of Atchison[16].

On the other hand, another approach was made to comprehend the neutron emission mechanism. As a result of parameter fitting, it was pointed out[17] that the preequilibrium process should be included in the INCE model. Nakahara[18] made an algorithm to take account of the preequilibrium process with use of a closed form exciton model. Ishibashi incorporated Gudima's closed form exciton model[19] in the microscopic reaction computation version of HETC-KFA2[20] as a multistep compound process[21] and revised the code as HETC-3STEP.[22] Kishida also included the exciton model into NUCLEUS and developed a code MCEXCITON[23] in which the exciton model calculation began when 2p1h state was formed in the cascade process.

With the rise of the interests on the nuclear data in the intermediate energy region, a benchmark calculation[24] was made with those INCE codes on the nuclide production cross sections. At this time, the benchmark calculation were carried out for double differential cross sections (DDXs) of (p,xn) and (p,xp) reactions of ^{208}Pb and ^{90}Zr at the energies of 25 to 1500 MeV.

In this paper, calculated results of the INCE code NUCLEUS and HETC-3STEP are shown and a discussion is made on the results. The calculated results of the cluster emission and the nuclide production cross section are also exhibited.

2. Calculational Procedures

2.1 NUCLEUS[11,12]

In NUCLEUS, the interaction between an incident particle and an intranuclear nucleon at the cascade process is treated as a collision of free particles in the degenerated Fermi sea. The target nucleus is divided into three regions having the relative nucleon densities of 0.9, 0.2 and 0.01 to the density at the center of the nucleus, respectively. The Fermi energy in each region is determined with the parametrized data. The constant value of 7 MeV is given to the intranuclear nucleons as the binding

energy in each region. The nuclear radii and the parameters to get the Fermi energy are stored in a data base.

In the simulation of a collision, the energies and the momentums of particles are calculated with the relativistic dynamics. The directional cosines are sampled from an angular distribution fitted to experimental data. The production of π meson via the excited state of a nucleon, Δ, is taken into account using the isobar model of Lindenbaum and Steinheimer[25]. In this code, it is assumed the Δ particle decays into a nucleon and a π meson immediately. The exclusion principle is applied by checking whether the kinetic energy of a struck particle exceeds the Fermi level including the binding energy. The cascade process is terminated when all particles reach to the cutoff energy which is set to the half values of Coulomb barrier above the Fermi level. Refraction and reflection of a particle on the surface of the target nucleus is not considered. The excitation energy U, mass number A and the charge number Z are stored in a file for the evaporation calculation to follow.

Before going to the evaporation stage, a check is made whether or not the fission reaction occurs using the probability for fission reaction P_f represented with the fission width Γ_f and the neutron emission width Γ_n :

$$P_f = \frac{1}{1+\Gamma_n/\Gamma_f} \quad , \tag{1}$$

$$\frac{\Gamma_n}{\Gamma_f} = \frac{4A^{2/3}a_f(U-Q_n)}{K_0 a_n[2a_f^{1/2}(U-E_f)^{1/2}-1]} \times \exp[2a_n^{1/2}(U-Q_n)^{1/2}-2a_f^{1/2}(U-E_f)^{1/2}] \quad , \tag{2}$$

$$K_0 = h^2/(8\pi^2 m r_0^2) \quad , \tag{3}$$

where Q_n the neutron binding energy, E_f the fission barrier height, a_n the level density parameter for neutron emission, a_f the one for fission, m the neutron mass and r_0 the nuclear radius. The ratio of the level density parameter a_f/a_n is determined by an expression fitted to the fission cross section data obtained by Il'inov et al.[26] for the incident proton energies of 150, 660 and 1000 MeV. The data of Il'inov and the ones of Kupryanov et al.[27] are employed to determine the fission barriers for the nuclides with A≤224 and for the ones with A≥225, respectively. The mass distribution of fission fragments for sub-actinide nuclides is calculated using a Gaussian distribution with the half width derived by Neuzil and Fairhall[28]. For actinide nuclides, it is calculated with the folded Gaussian distribution with the parameters obtained by fitting to the data of Grass et al.[29] for the α-induced fission of ^{239}Pu. The charge of the fission fragment is determined by a Gaussian distribution with the parameters obtained by Pik-Pichak and Strutinskii[30] for the mass of given fragments.

In the evaporation stage, the 6 particles, n, p, d, t, ^{3}He and α, are taken into account. The probability for emission of a particle is given by the statistical model of Weisskopf-Ewing[31]:

$$P_x(\varepsilon)\,d\varepsilon = (2S_x+1)\,\omega_x(E)\,\varepsilon\,\sigma_{cx}(\varepsilon)\,d\varepsilon \quad , \tag{4}$$

where S_x the spin of particle x, ε the kinetic energy of particle x, $\omega_x(E)$ the level density and $\sigma_{cx}(\varepsilon)$ the inverse reaction cross section for emission of particle x from the residual nucleus. The level density is given by

$$\omega_x(E) = \omega_0 \exp[2\sqrt{a(E-\delta)}] \quad , \tag{5}$$

$$E = U - Q_x - \epsilon \quad , \tag{6}$$

where a is the level density parameter, δ the pairing energy and Q_x the binding energy of particle x. Q_x is calculated with the Cameron's mass formula[32]. For the level density parameter, an expression derived by LeCouteur[33] is employed:

$$a = \frac{A}{B}\left(1 + Y\frac{\Delta^2}{A^2}\right) \quad , \tag{7}$$

where $\Delta = A - 2Z$, B=8 MeV, Y=1.5 MeV. In the evaporation process, neither the conservation of angular momentum nor discrete levels of a nucleus is taken into account. In addition, the gamma-ray emission is not considered.

2.2 HETC-3STEP[22]

In HETC-3STEP, the computation model is the same as in NUCLEUS except that the preequilibrium process and the Atchison's high energy fission model[15] are included. The preequilibrium process is analyzed with Gudima's closed form exciton model[19]. Gudima et al. applied the exciton model from 2p1h state regardless of preceding cascade process and adopted forward peaked angular distribution. From a detailed study[34] on the neutron emission spectra with a moving source model, however, the angular distribution of the neutrons from the preequilibrium process has been found isotropic. So the cascade is regarded as the limit of the multistep direct process and the following preequilibrium process as the multistep compound process.

In connection with the inclusion of the preequilibrium process, the calculational procedure is changed as follows. The cut-off energy given by the expression of $f(E_c) = 2E_0^{-1}(1 - E_c/E_0)$ is used in the cascade process, where E_c has been sampled randomly in the range from 0 to 40 MeV. The value of 40 MeV has been found to be consistent with the decomposed cascade spectra. For protons, the cut-off energy E_c is sampled in the same manner, but if the sampled value comes below the Coulomb barrier height, the value is substituted by this barrier energy. The transition probabilities for the increase, the unchangeness and the decrease of the exciton number, which are indicated as $\lambda+$, $\lambda 0$, and $\lambda-$, respectively, are multiplied by factor F represented as

$$F = max(0.2,\ 3.5 - 13A^{-1/2}) \quad . \tag{8}$$

The factor was determined so that the calculated neutron spectra could agree with the preequilibrium component of the decomposed neutron spectra for a variety of targets from C to Pb. The decomposed neutron spectra are shown in Fig.1. The preequilibrium process has been terminated on the condition that the number of exciton comes to $(2gE)^{1/2}$ or 15. Here, g is the single particle level density. The angular distribution of an emitted particle is made to be isotropic.

It should be noted that HETC-3STEP employs the mass dependent level density parameter deduced by Baba[35] and the excitation energy dependent Coulomb barrier. In Fig. 2, the mass dependent level density parameter is shown with the ones obtained with the value of A/8. As for the Coulomb barrier, it is given as

$$V_x = \frac{Z_x Z e^2}{R + R_x} \quad . \tag{9}$$

In HETC-3STEP, the value V_x varies with the excitation energy as $1/(1+0.005U/Z)$, where U is the excitation energy and Z the charge number of an ejectile. The influences of these parameters are discussed in the following section.

3. Results and Discussions

3.1 Reaction Cross Section

In NUCLEUS and HETC-3STEP, the reaction cross section, σ_r, is obtained by

$$\sigma_r = \sigma_g \times \frac{N_r}{N_T} \quad , \tag{10}$$

where σ_g is the geometrical cross section, N_r the number of non-elastic events and N_T the number of total events. In Fig.3, calculated reaction cross sections for the proton incidence on ^{208}Pb and ^{90}Zr are displayed with the values obtained with the systematics derived by Pearlstein[36] . With the increase of incident energy, the reaction cross section evaluated by the systematics decreases and almost agrees with the ones obtained by the INCE codes in the energy region above 100 MeV. At several tens of MeV, the calculated results become smaller by about 20% than by the systematics for ^{208}Pb. Somewhat smaller discrepancy is seen for the result on ^{90}Zr. This means that the approximation with the constant geometrical cross section is not appropriate in the several tens of MeV region, whereas it is proved to be reliable above 100 MeV.

Since the mean free path of the travelling particle in a matter is determined based on this constant geometrical cross section in the transport code such as NMTC/JAERI and HETC-KFA2, the underestimation of the reaction cross section may lead to the overestimation of the mean free path of the neutrons with several tens of MeV. In order to improve the underestimation of the reaction cross section, some correction should be made. It is considered that the inclusion of energy dependent Nucleon-Nucleon collision cross section might be effective as the correction.

3.2 Parameter Dependence

As is described in the previous section, different values are employed on the Coulomb barrier and on the level density parameter in NUCLEUS and HETC-3STEP. Here, the influence of these parameters on the nucleon spectra is examined with NUCLEUS by substituting the default values of the Coulomb barrier and the level density parameter for the ones employed in HETC-3STEP. In Figs. 4 and 5, proton and neutron DDX at 30° are shown for 800 MeV proton incidence on ^{208}Pb, respectively. As is displayed with a dashed lines in Fig.4, the use of an excitation energy dependent Coulomb barrier enables the code to predict the proton emission to lower energy than the Coulomb barrier of about 8 MeV.

As for the level density, one can easily deduce from Eq.(5) that the use of Baba's level density parameter would suppress the number of the evaporation particles from ^{208}Pb in comparison with the case using the default value of $A/8$. For the 800 MeV proton incidence, it is observed in Fig. 4 that the yield of protons decreases to 50% or more by replacing the value $A/8$ into the one deduced by Baba. The yield of evaporation neutrons also diminishes by 20 to 50%. It is suggested from these results that a careful attention should be paid on the choice of this parameter.

3.3 Neutron DDX

In Figs. 6 to 19, the calculated neutron DDXs are compared with the experimental ones[37-43] for ^{208}Pb and ^{90}Zr at incident energies from 25 to 1500 MeV. At incident energies up to 160 MeV, it is observed in common that NUCLEUS underestimates the experimental neutron DDX above 10 MeV at the backward angles greater than 90°. As the incident energy decreases, this tendency becomes more significant. For a lower incident energy such as 25 and 45 MeV, the degree of underestimation reaches to one to two figures. On the contrary, good agreements are obtained between NUCLEUS and the experiment at the intermediate angles of 25° to 60°, although the agreement becomes somewhat worse at 25 and 45 MeV. At the very forward angle of 11°, NUCLEUS overestimates the highest energy component of the neutron spectra by a factor of 5 or more, which comes from the quasi-elastic reaction. However, the code underestimates the continuum part following the quasi-elastic part.

It seems that the neutron emission to forward angle is evaluated too large in the intranuclear cascade process for low energy incidence. In order to simulate the backward neutron emission more accurately, it may be necessary to take the refraction and the reflection of a particle on the surface of

the target nucleus into account. Preliminary calculations have been carried out with the code ISOBAR[44] which has an option to take the refraction and the reflection in the intranuclear cascade calculation. The results are shown in Fig. 20 and 21 for the 80 and 256 MeV proton incidence, respectively. Here, the normalization to the cross section was made with the reaction cross section obtained by NUCLEUS. It is clearly seen that the fraction for backward neutron emission increases and reproduces the experimental data well although the high energy component of the calculated backward neutron DDX is too high. It is observed from Fig. 21 that the inclusion of the refraction and the reflection improves the discrepancy on the quasi-elastic peak and the continuum part following the peak well together with the backward component. Since the ISOBAR code treats only the cascade process, it is of interest to make calculations including the evaporation process to investigate the effect of the refraction and the reflection more in detail.

As far as concerned with HETC-3STEP, the code successfully improves the outstanding underestimation of NUCLEUS for the neutron emission to backward angles and achieves excellent agreements with the experimental data for both ^{208}Pb and ^{90}Zr in the energy range of 45 to 160 MeV. As is seen in Fig. 6, the results of HETC-3STEP are too large compared to the experimental data at 25 MeV. In comparison with another data for ^{208}Pb at incident energy of 25.5 MeV, however, it has been confirmed that HETC-3STEP reproduces the backward neutron spectra fairly well.[45] Therefore, it is considered that HETC-3STEP is applicable to the neutron cross section calculations at several tens of MeV and is concluded that the inclusion of preequilibrium process improves the accuracy of INCE model in the energy region below 160 MeV.

For the incident energy above 256 MeV, it is observed in Figs. 14 to 19 that there is little difference between the calculated results of NUCLEUS and HETC-3STEP even at the backward angles although a difference is seen in the evaporation component. This result is attributed to the following phenomenon. As the incident energy increase, the number of nucleons which is involved in the intranuclear cascade process increases so that the excitons close to the termination condition have been already produced at an initial stage of the preequilibrium process. As for the difference between the evaporation component, this is caused by the use of different parameters in the evaporation calculation. Judging from the neutron spectra shown in Figs. 14 to 19, the level density parameter deduced by Baba seems to be more suitable than the one given by A/8.

For 256 and 800 MeV, two sets of the experimental data are shown for the Pb target. The major causes of the difference are due to the detector efficiencies and the background subtraction technique.[41] The calculated results are in good agreements with the experimental data by LANL[40,42] rather than the ones by Hamburg University[41]. At the incident energy of 1500 MeV, good agreements are obtained between the calculation and the experiment in the energy region above 3 MeV at every angles. For the incident energy from 256 to 1500 MeV, the INCE model predicts the backward neutron emission fairly well. On the very forward neutron spectrum at 7.5°, the calculation codes cannot reproduce the quasi-elastic peak and the following continuum part as well as the case of 160 MeV incidence. This may indicate the limit of the approximation of two-body collision of free particles in the intranuclear cascade process. As a whole, however, it is considered that the INCE model has good accuracy enough to evaluate the neutron DDX at incident energies above 256 MeV.

3.4 Proton DDX

The results on the proton DDXs are shown in Figs. 22 and 23 for 80 MeV proton incidence on ^{90}Zr and 200 MeV proton on ^{197}Au. For 80 MeV proton incidence, NUCLEUS predicts the proton DDX at medium angles fairly well, but underestimates the backward proton spectra by one figure or more. On the contrary, HETC-3STEP improves the underestimation of NUCLEUS on the backward proton spectra and is in good agreement with the experimental data[46]. For the 200 MeV proton incidence, however, the proton yields estimated by HETC-3STEP does not increase as in the case of 80 MeV incidence, so that the calculated results are still lower than the experimental results[47].

In both cases, there exist the differences of a factor of 2 to 3 in the evaporation component of the proton spectra between NUCLEUS and HETC-3STEP due to the difference of the parameters in the evaporation calculation. Because the lack of available experimental data at the low energy region,

it cannot be concluded which results are better, yet. As for HETC-3STEP, the parameters employed in the preequilibrium process was determined by the neutron spectra alone. It is found, therefore, that the parameters are able to applicable to the estimation of the proton emission reaction.

3.5 Cluster DDX

In Figs. 24 and 25, the calculated deuteron and alpha DDXs respectively are compared with the experimental results[48] of ^{90}Zr for the 90 MeV proton incidence. In NUCLEUS, since the cluster emission is considered only in the evaporation process, the code evaluates the cluster emission up to several MeV. As far as the energy of cluster is concerned, HETC-STEP gives the similar results to NUCLEUS although cluster emission is taken into account in the preequilibrium process. It should be noted that the HETC-3STEP estimates the cluster emission much larger than NUCLEUS by about a factor of 5. Comparing with the results of the neutron and the proton DDXs, it is difficult to explain the increase of the cluster yields by the use of HETC-3STEP. It may be necessary to examine the calculational scheme for cluster emission in detail.

It is clearly illustrated in Figs. 24 and 25 that there are contributions having forward peak angular distribution from the direct process in both the experimental deuteron and alpha spectra. Therefore, it is necessary to include another process into the INCE model to estimate those components, appropriately.

3.6 Nuclide Production Cross Section

Both NUCLEUS and HETC-3STEP give the information on the nuclide production. In Figs. 26 to 30, the calculated nuclide production cross sections for proton incidence on ^{nat}Fe are shown with the experimental data[49-51]. For the ^{56}Co production, both of the calculated results give larger values of about a factor of two than the experiment. This is consistent with the results that the quasi-elastic peak is overestimated in the neutron DDXs. As the mass number of the products gets apart from the target nucleus, the difference between NUCLEUS and HETC-3STEP becomes more obvious. It seems, however, the consistency is not observed in the difference between the calculated results and the experimental data for those nuclides.

It should be noted that the there are many elements which affect the nuclide production. Those are the mass formula to calculate the binding energy, the inclusion of cluster emission from direct process, the fission product yield dependent on some parameters and so on. Consequently, it is difficult to evaluate the accuracy of INCE model in the nuclide production rigidly. Roughly speaking, the INCE model is able to evaluate the nuclide production cross sections for ^{nat}Fe within twice as large as the experiment at present.

4. Conclusions

Benchmark calculations were carried out with the codes NUCLEUS and HETC-3STEP. Both codes are based on the INCE model and the latter can take the preequilibrium process into account. It is concluded from the calculations that the code NUCLEUS can evaluate the neutron DDXs fairly well at the high incident energies from 256 to 1500 MeV except for the one at the very forward angle. HETC-3STEP gives higher accuracy than NUCLEUS by including the preequilibrium process and makes it possible to evaluate the neutron DDXs quite well at lower incident energy below 160 MeV although there remains some discrepancies at the forward angles. It has been found that the code HETC-3STEP also improves the proton DDX at energies of 80 MeV.

Form the view point of using the INCE model without the preequilibrium process, it is suggested from the preliminary calculation that inclusion of the refraction and the reflection on the surface of the target has a possibility to correct the angular distribution of the cascade particle and to improve the discrepancies at both the forward and the backward angles.

At several tens of MeV, the reaction cross section is not estimated correctly. In order to calculate the nuclear reaction with the INCE model strictly in this energy region, it is necessary to include the energy dependence into the geometric cross section of the target nucleus. Moreover, it is

also recommended to take some new computation models into account to predict the cluster emission more accurately. Those approaches will lead to improve the accuracy of NUCLEUS and HETC-3STEP in the nuclide production cross sections. At present, it is found that those codes can predict the cross sections within twice as large as the experiment.

References

(1) C.D.Bowman et al., Nucl. Instr. and Meth. in Phys. Res. **A320**, (1992), 336.
(2) H.Takahashi and H.Rief, "Concept of Accelerator Based Transmutation Systems", Proc. of Specialists' Mtg. on Accelerator-Based Transmutation, PSI, Villigen, Switzerland, Mar. 24-26, 1992, p2.
(3) H.Takizuka, T.Nishida, H.Takada, S.Meigo and M.Mizumoto, "Conceptual Design Study of an Accelerator-based Actinide Transmutation Plant with Sodium-cooled Solid Target/Core", Proc. of OECD/NEA Mtg. on Int. Information Exchange Program on Partitioning and Transmutation of Actinides and Fission Products, November 11-13, 1992, ANL Argonne, p398 (1993).
(4) H.Takashita, H.Harada, H.Takahashi and A.Aronson, "Transmutation of Long-Lived Radioactive Nuclides", Proc. of Int. Conf. and Exhibition Future Nuclear System: Emerging Fuel Cycles and Waste Disposal Options (Grobal '93), September 12-17, 1993, Seattle, Washington, p797.
(5) I.V.Chuvilo, G.V.Kiselev, B.R.Bergelson and B.P.Kochurov,"Nuclear Fuel Cycle Using Nuclear Power facilities Based on Subcritical Blankets Driven by the Proton Accelerator", ibid. p924.
(6) Proc. Information Mtg. Accelerator Breeding, Brookhaven, New York, June 18-19, 1977, CONF-770107, National Technical Information Service (1977).
(7) A.J.Koning,"Requirements for an Evaluated Nuclear Data File for Accelerator Based Transmutation", NEA/NSC/DOC(93)6, (1993).
(8) A.J.Koning, "Review of High Energy Data and Model Codes for Accelerator-Based Transmutation", NEA/NSC/DOC(92)12 (1992).
(9) H.W.Bertini, Phys. Rev. **188**, 174 (1969).
(10) L.W.Dresner, "EVAP - A Fortran Program for Calculating the Evaporation of Various Particles from Excited Compound Nuclei", ORNL-TM-196, (1962).
(11) Y.Nakahara and T.Tsutsui, JAERI-M 82-198, (1982) (in Japanese).
(12) T.Nishida, Y.Nakahara and T.Tsutsui, JAERI-M 86-116, (1986) (in Japanese).
(13) Y.Nakahara, J. Nucl. Sci. Technol. **20**, 511 (1983).
(14) T.Nishida and Y.Nakahara, Kerntechnik. **50**, 193 (1987).
(15) T.Nishida, H.Takada, Y.Nakahara, T.Takizuka N.Yoshizawa and S.Iwai, "Benchmark Study on the Computational Model in the Accelerator-Based Transmutation Simulation Code", Proc. of Specialists' Mtg. on Accelerator-Based Transmutation, PSI, Villigen, Switzerland, March 24-26, 1992, p535.
(16) F.Atchison, "Spallation and Fission in Heavy Metal Nuclei under Medium Energy Proton Bombardment", Proc. of Mtg. on Targets for Neutron Beam Spallation Source, KFA-Jülich, Germany, June 11-12, 1979, Jül-Conf34, (1980).
(17) K.Tsukada and Y.Nakahara, Atomkernenergie Kernteknik, **44**, 186 (1984).
(18) Y.Nakahara and T.Nishida, JAERI-M 86-074 (1986).
(19) K.K.Gudima, S.G.Mashnik, and V.D.Toneev, Nucl. Phys. **A401**, 329 (1983).
(20) P.Cloth, D.Filges, R.D.Neef, G.Sterzenbach, Ch.Reul, T.W.Armstrong, B.L.Colborn, B.Anders and H.Brückmann, "HERMES A Monte Carlo Program System for Beam-Materials Interaction Studies", Jül-2203 (1988).
(21) H.Feshbach, A.Kerman and S.Koonin, Ann. Phys. **125**, 429 (1980).
(22) K.Ishibashi, N.Yoshizawa, H.Takada and Y.Nakahara, "High Energy Transport Code HETC-3STEP Applicable to Incident Energies Below 100 MeV", Proc. of Int. Conf. on Nucl. Data for Sci. and Technol., Gatlinburg, Tennessee, May 9-13, 1994, to be published.
(23) N.Kishida and H.Kadotani, "Exciton Model Analysis of Double Differential Neutron Production Cross Sections for 113 MeV Protons", Proc. of Int. Conf. on Nucl. Data for Sci. and Techol., Jülich, May 13-17 1991, p1005.

(24) T.Fukahori, S.Chiba, H.Takada, N.Kishida, Y.Watanabe, and N.Yamamuro, JAERI-M, to be published.
(25) R.M.Steinheimer and S.J.Lindenbaum, Phys. Rev. **105**, 1874 (1957), **109**, 1723 (1958), **123**, 333 (1961).
(26) A.S.Il'inov, E.A.Cherpanov and S.E.Chigrinov, Sov. J. Nucl. Phys. **32**, 166 (1980).
(27) V.M.Kupriyanov, et al., Sov. J. Nucl. Phys. **32**, 184 (1980).
(28) F.F.Neuzil and A.W.Fairhall, Phys. Rev. **129**, 2705 (1963).
(29) R.A.Grass et al.,Phys. Rev. **104**, 404 (1956).
(30) G.A.Pik-Pichak and V.M.Strutinskii, "Physic of Nuclear Fission", p2, edited by N.A.Perfilov and V.S.Eismont, Israel Program for Scientific Translation, 1964.
(31) J.M.Blatt and V.F.Weisskopf,"Theoretical Nuclear Physics", Wiley and Sons. 1952.
(32) A.G.W.Cameron, Canad. J. Phys., **35**, 1021 (1957).
(33) K.J.LeCouteur, Proc. Phys. Soc. (London), **A63**, 259 (1950).
(34) K.Ishibashi, K.Higo, S.Sakaguchi, Y.Matsumoto, Y.Wakuta, H.Takada, T.Nishida, Y.Nakahara and Y.Kaneko, J. Nucl. Sci. and Technol. **29**, 499 (1992).
(35) H.Baba, Nucl. Phys. **A159**, 625 (1970).
(36) S.Pearlstein, Nucl. Sci. Eng. **95**, 116 (1987).
(37) R.R.Doering, D.M.Patterson and A.Galonsky, Phys. Rev. **C12**, 378 (1975).
(38) M.Trabandt, W.Scobel, M.Blann, B.A.Pohl, R.C.Byrd, C.C.Foster and R.Bonetti, Phys. Rev. **C39**, 452 (1989).
(39) W.Scobel, M.Trabandt, M.Blann, B.A.Pohl, B.R.Remington, R.C.Byrd, C.C.Foster, R.Bonetti, C.Chiesa and S.M.Grimes, Phys. Rev. **C41**, 2010 (1992).
(40) M.M.Meier, C.A.Goulding, G.L.Morgan. and J.Ullmann, Nucl. Sci. and Eng. **104**, 339 (1990).
(41) S.Stamer, W.Scobel, W.B.Amian, R.C.Byrd, R.C.Haight, J.L.Ullmann, R.W.Bauer, M.Blann, B.A.Pohl, J.Bisplinghoff and R.Bonetti, Phys. Rev. **C47**, 1647 (1993).
(42) W.B.Amian, B.C.Byrd, C.A.Goulding, M.M.Meier, G.L.Morgan, C.E.Moss and D.A.Clark, Nucl. Sci. Eng. **112**, 78 (1992).
(43) K.Ishibashi, T.Nakamoto, N.Matsufuji, N.Shigyo, K.Maehata, Y.Wakuta, Y.Watanabe, H.Takada, S.Meigo, S.Chiba, M.Numajiri and T.Nakamura, "Measurement of Neutron-Production Double Differential Cross Sections for Incident Protons of 0.8, 1.5 and 3.0 GeV.", Proc. of Int. Conf. on Nucl. Data for Sci. and Technol., Gatlinburg, Tennessee, May 9-13, 1994, to be published.
(44) K.Chen, Z.Fraenkel, G.Friedlander, J.R.Grover, J.M.Miller and S.Shimamoto, Phys. Rev. **166**, 949 (1968), **109**, 1723 (1958), **123**, 133 (1961).
(45) K.Ishibashi, H.Takada, Y.Yoshizawa, N.Matsufuji, T.Nakamoto, Y.Wakuta and Y.Nakahara, "Inclusion of Preequilibrium Calculation into High Energy Transport Code", Proc. of 12th Mtg. on Int. Collaboration on Advanced Neutron Sources, (ICANS XII), May, 24-28, 1993, Abington, U.K., Rutherford Appleton Laboratory Report 94-025, Vol.2, T44 (1994).
(46) A.A.Cowley, A.van Kent, J.J.Lawlie, S.V.Förtsch, D.M.Whitthal, J.V.Pilcher, F.D.Smit, W.A.Richter, R.Lindsay, I.J.van Heerden, R.Bonetti and P.E.Hodgson, Phys. Rev. **C43**, 678 (1991).
(47) A.A.Cowley, S.V.Förtsch, J.J.Lawlie, D.M.Whitthal, F.D.Smit and J.V.Pilcher, Z. Phys. **A336**, 189 (1990).
(48) J.R.Wu, C.C.Chang and H.D.Holmgren, Phys. Rev. **C19**, 698 (1979).
(49) R.Michel and R.Stück, J. Geophys. Res. **V89**, B673 (1984).
(50) R.Michel, G.Brinkmann, H.Weigel and W.Herr, Nucl. Phys. **A322**, 40 (1979).
(51) R.Michel, B.Dittrich, U.Herpers, F.Peiffer, T.Schiff, P.Cloth, P.Dragovitch and D.Filges, Analist, **V114**, 287 (1989).

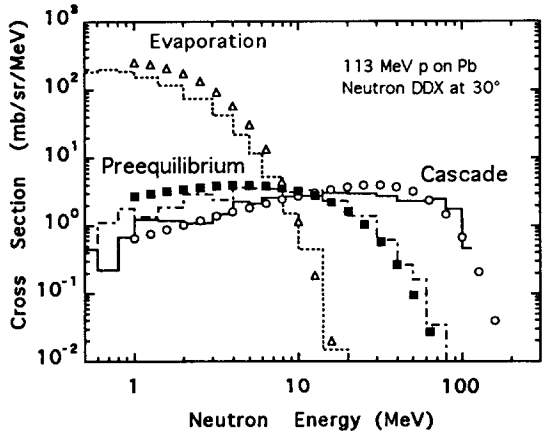

Fig. 1. Neutron spectra decomposed by the moving source model (marks) and results of HETC-3STEP (lines) for 113 MeV proton incidence on Fe target.

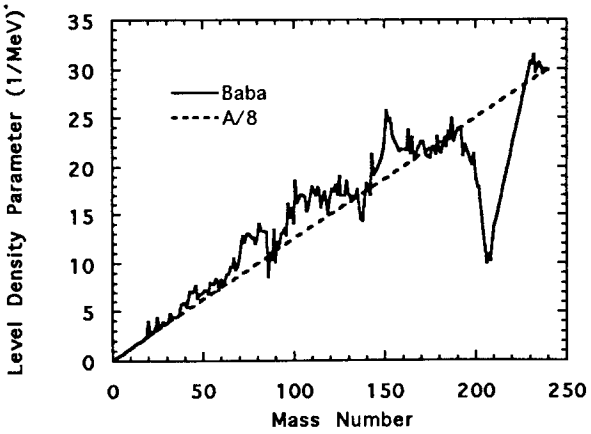

Fig. 2. Comparison of level density parameter.

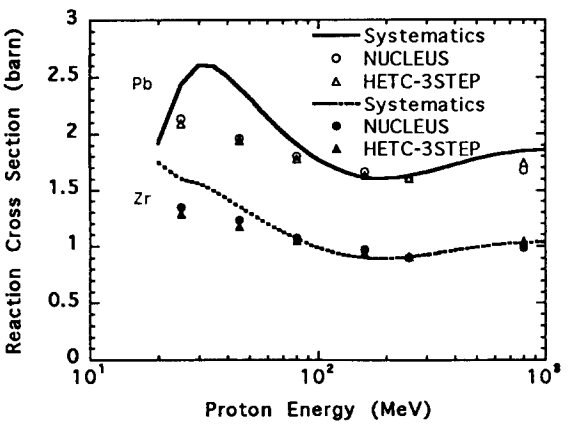

Fig. 3. Reaction Cross Sections for proton incidence on ^{208}Pb and ^{90}Zr. Open circle and triangle indicate the results of NUCLEUS and HETC-3STEP, respectively. Lines are for Pearlstein's systematics.

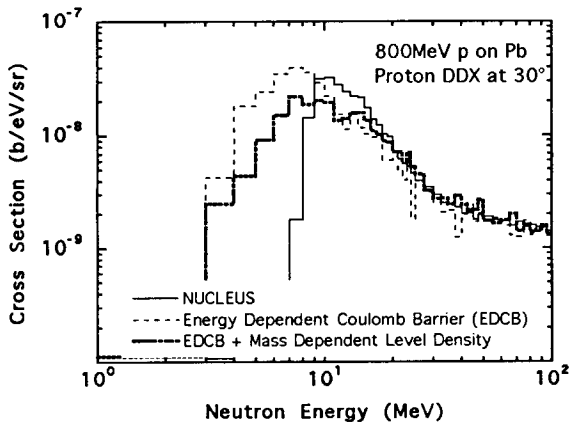

Fig. 4. Proton DDX at 30° for 800 MeV proton incidence on ^{208}Pb. Solid line indicates the result of NUCLEUS. Dashed and dotted lines represent the results with the use of excitation energy dependent Coulomb barrier and the ones including baba's level density parameter.

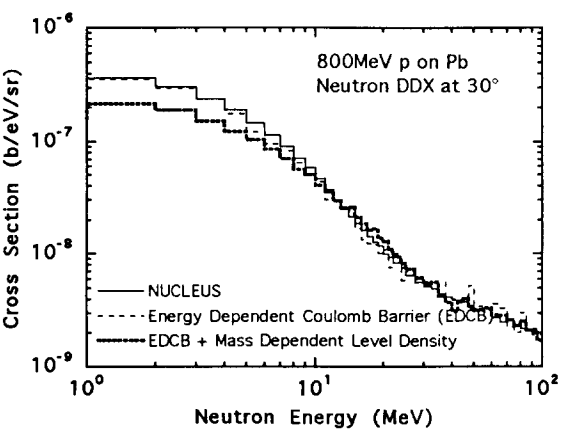

Fig. 5. Neutron DDX at 30° for 800 MeV proton incidence on ^{208}Pb. The lines are the same as for Fig.4.

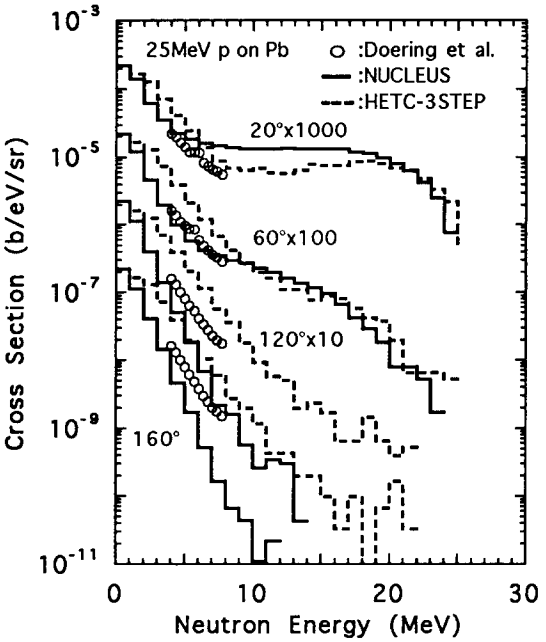

Fig. 6. Experimental[37] and Calculated Neutron differential cross sections of ^{208}Pb for 25 MeV proton Incidence. The Solid and the dotted lines indicate the results of NUCLEUS and HETC-3STEP, respectively.

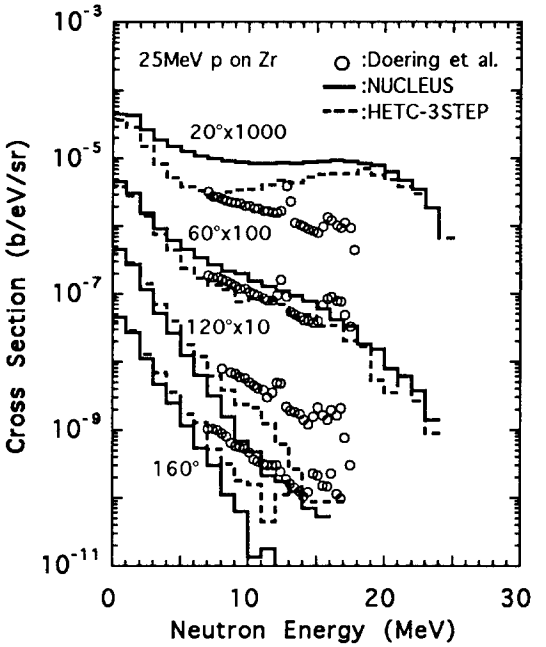

Fig. 7. Experimental[37] and Calculated Neutron differential cross sections of ^{90}Zr for 25 MeV proton Incidence. The lines are the same as for Fig.6.

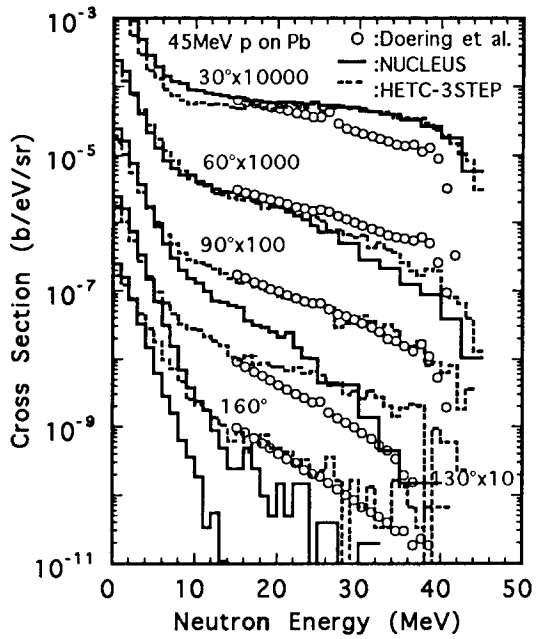

Fig. 8. Experimental[37] and Calculated Neutron differential cross sections of ^{208}Pb for 45 MeV proton Incidence. The lines are the same as for Fig.6.

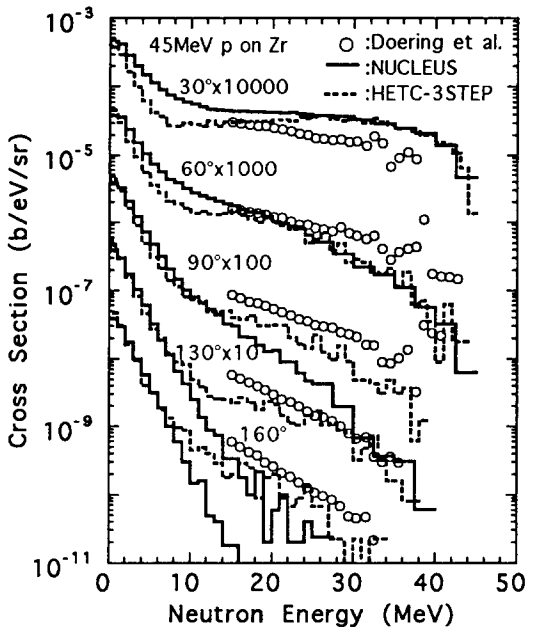

Fig. 9. Experimental[37] and Calculated Neutron differential cross sections of ^{90}Zr for 45 MeV proton Incidence. The lines are the same as for Fig.6.

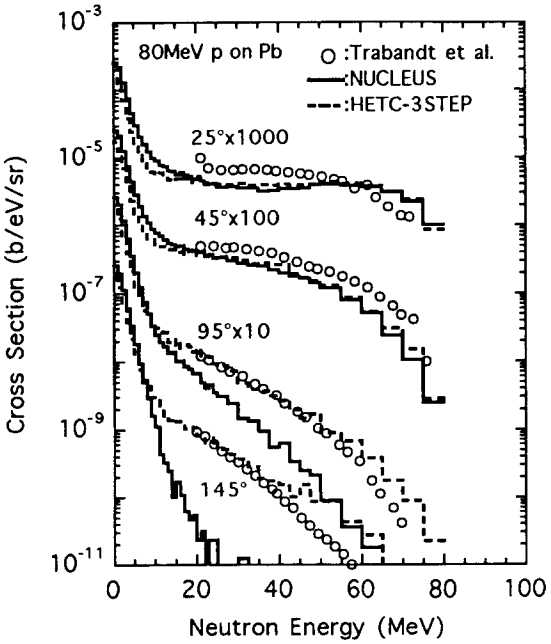

Fig. 10. Experimental[38] and calculated neutron differential cross sections of ^{208}Pb for 80 MeV proton incidence. The lines are the same as for Fig.6.

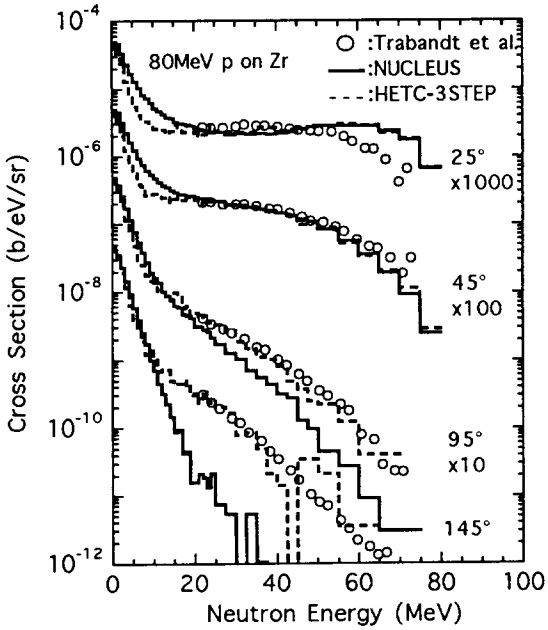

Fig. 11. Experimental[38] and calculated neutron differential cross sections of ^{90}Zr for 80 MeV proton incidence. The lines are the same as for Fig.6.

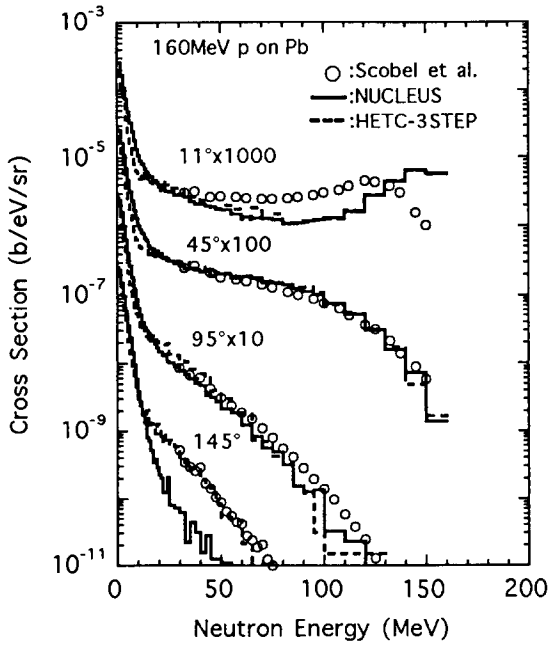

Fig. 12. Experimental[39] and calculated neutron differential cross sections of ^{208}Pb for 160 MeV proton Incidence. The lines are the same as for Fig.6.

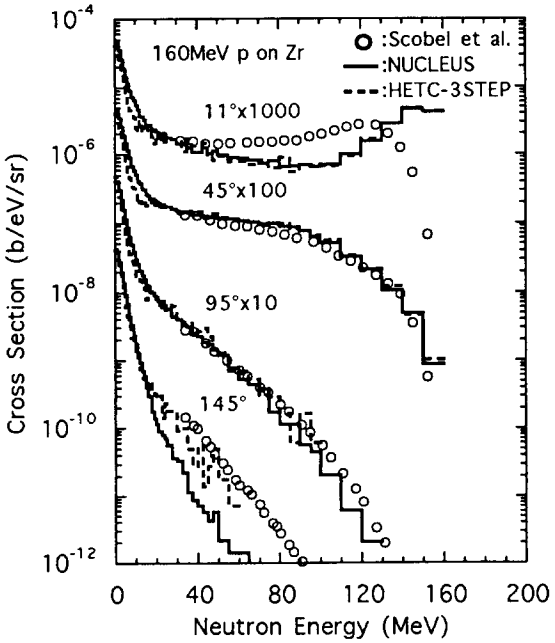

Fig. 13. Experimental[39] and calculated neutron differential cross sections of ^{90}Zr for 160 MeV proton incidence. The lines are the same as for Fig.6.

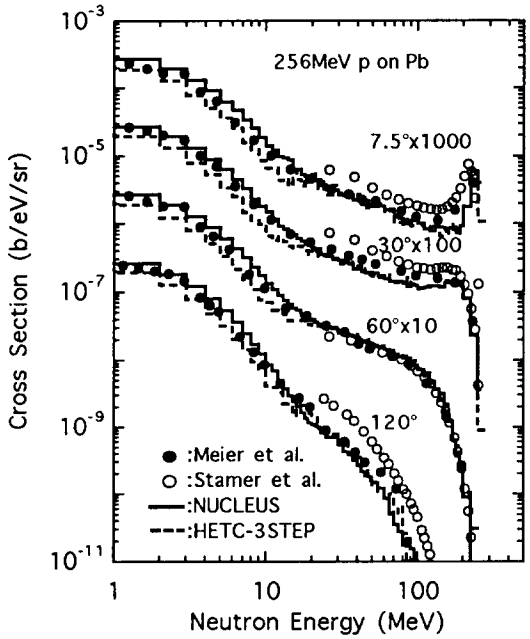

Fig. 14. Experimental[40,41] and calculated neutron differential cross sections of ^{208}Pb for 256 MeV proton incidence. The lines are the same as for Fig.6.

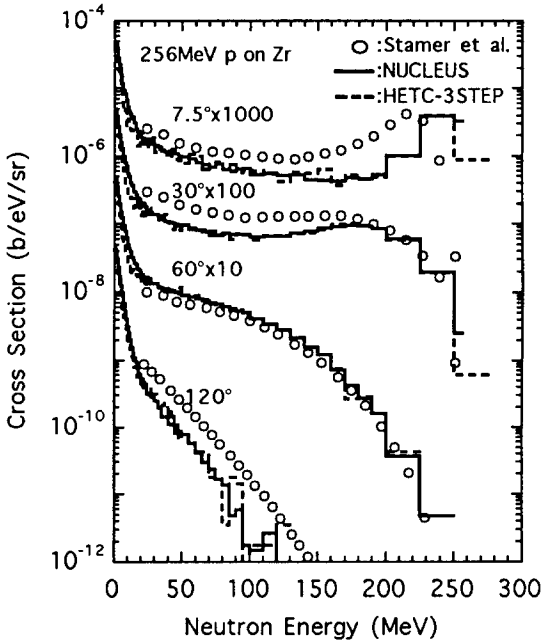

Fig. 15. Experimental[41] and calculated neutron differential cross sections of ^{90}Zr for 256 MeV proton incidence. The lines are the same as for Fig.6.

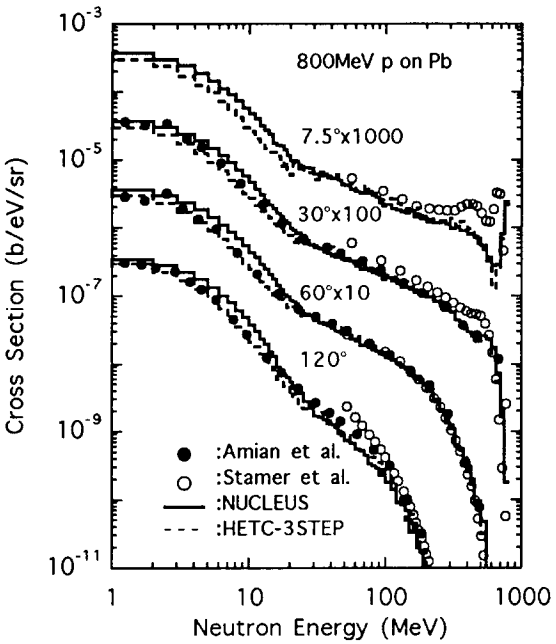

Fig. 16. Experimental[41,42] and calculated neutron differential cross sections of ^{208}Pb for 800 MeV proton incidence. The lines are the same as for Fig.6.

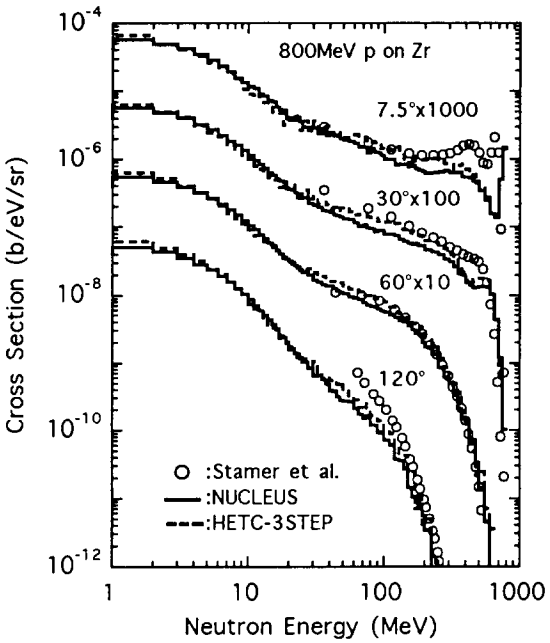

Fig. 17. Experimental[41] and calculated neutron differential cross sections of ^{90}Zr for 800 MeV proton incidence. The lines are the same as for Fig.6.

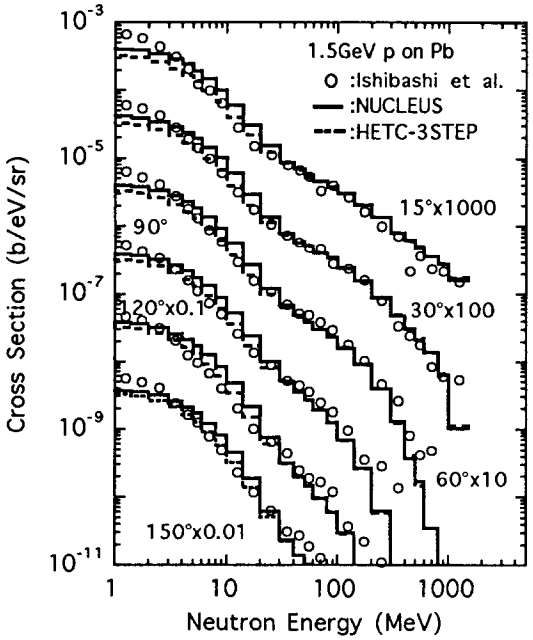

Fig. 18. Experimental[43] and calculated neutron differential cross sections of ^{208}Pb for 1500 MeV proton incidence. The lines are the same as for Fig.6.

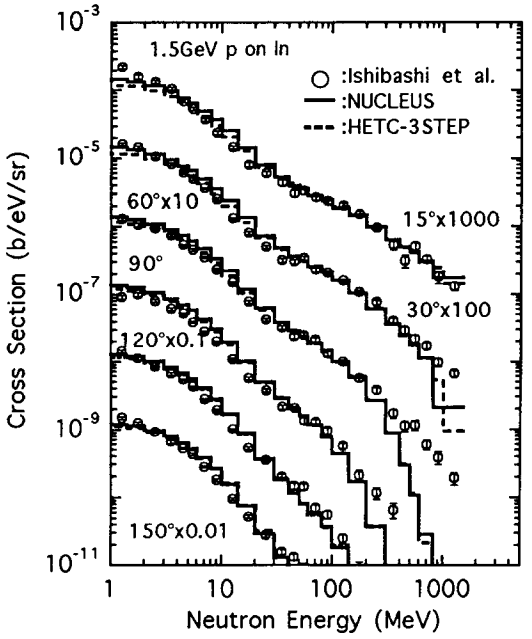

Fig. 19. Experimental[43] and calculated neutron differential cross sections of ^{nat}In for 1500 MeV proton incidence. The lines are the same as for Fig.6.

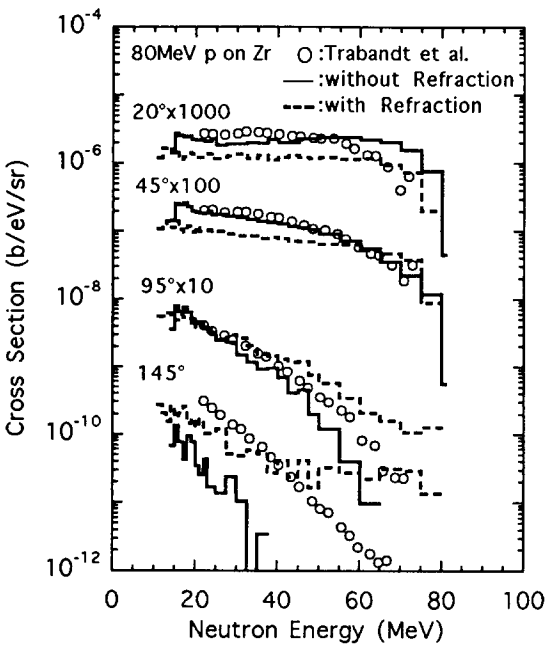

Fig. 20. Experimental[38] and calculated neutron differential cross sections of ^{90}Zr for 80 MeV proton incidence. The dotted and the solid lines indicate the results of ISOBAR[44] with and without the option of refraction and reflection, respectively.

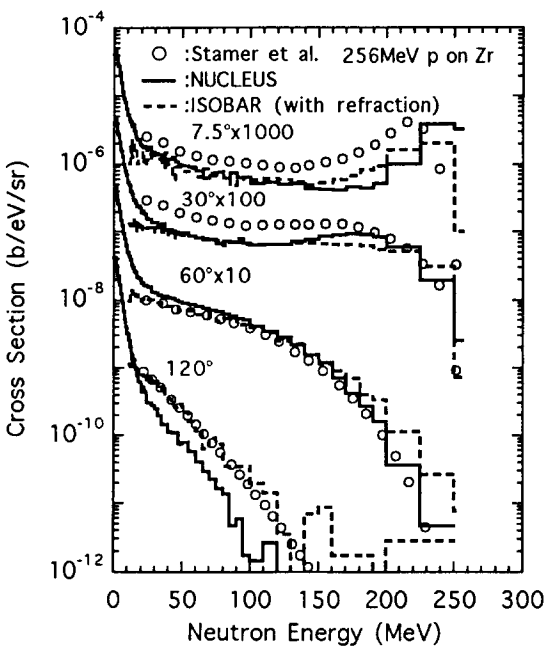

Fig. 21. Experimental[41] and calculated neutron differential cross sections of ^{90}Zr for 256 MeV proton incidence. The solid and the dotted lines indicate the results of NUCLEUS and ISOBAR[44] with the option of refraction and reflection, respectively.

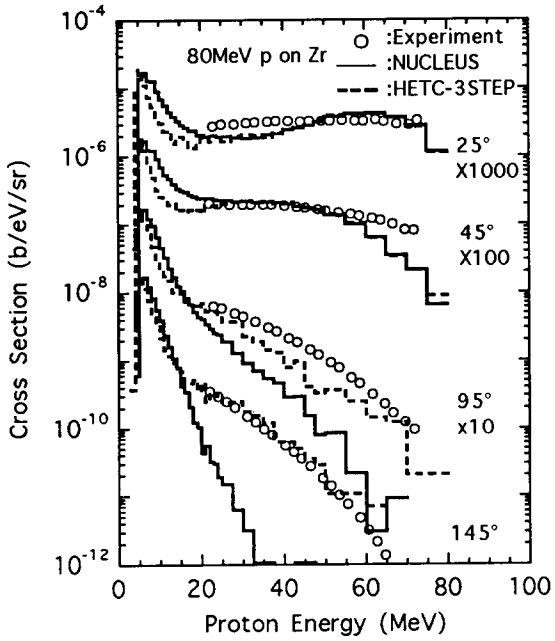

Fig. 22. Experimental[46] and calculated proton differential cross sections of ^{90}Zr for 80 MeV proton incidence. The lines are the same as for Fig.6.

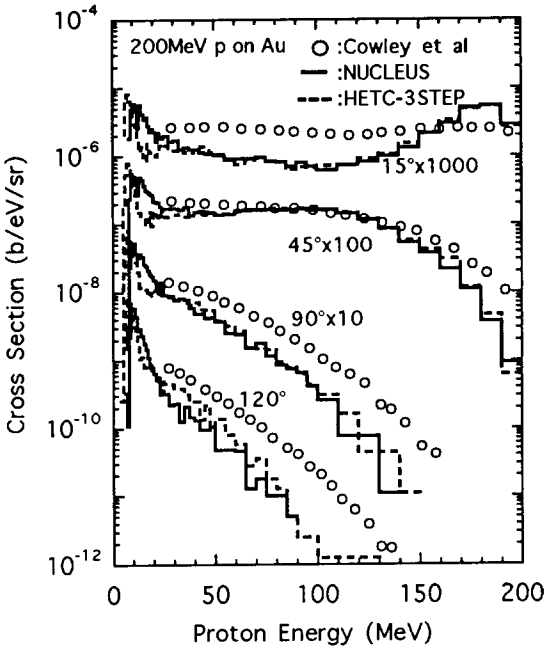

Fig. 23. Experimental[47] and calculated proton cross sections of ^{197}Au for 200 MeV proton incidence. The lines are the same as for Fig.6.

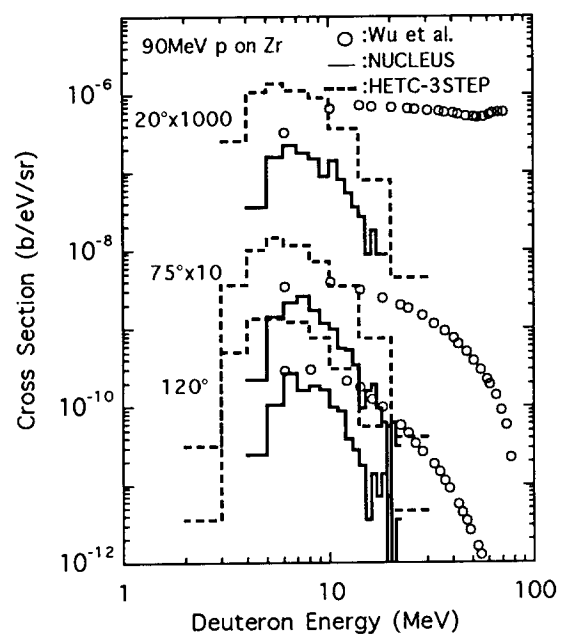

Fig. 24. Experimental[48] and calculated deuteron cross sections of ^{90}Zr for 90 MeV proton incidence. The lines are the same as for Fig.6.

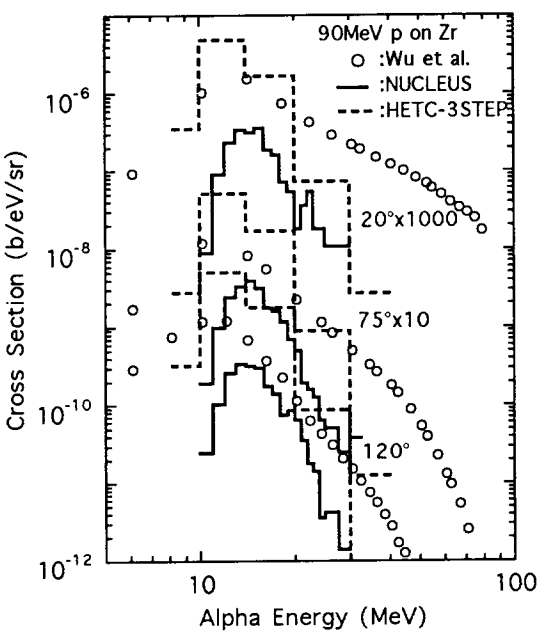

Fig. 25. Experimental[48] and calculated alpha particle differential cross sections of ^{90}Zr for 90 MeV proton incidence. The lines are the same as for Fig.6.

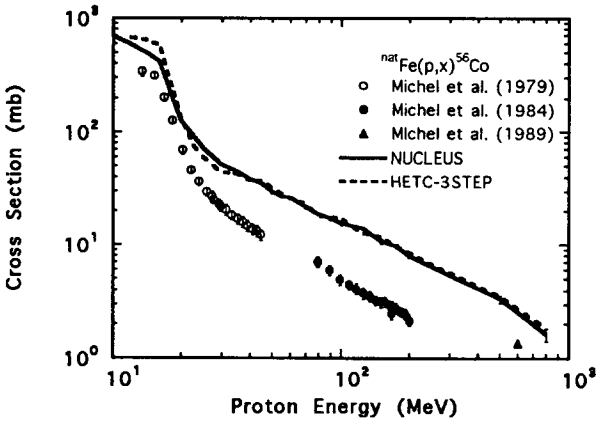

Fig. 26. Experimental[49-51] and calculated production cross section of ^{56}Co for proton incidence on ^{nat}Fe. The lines are the same as for Fig.6.

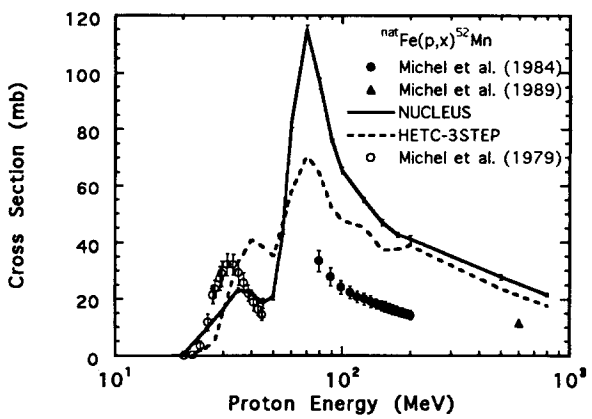

Fig. 27. Experimental[49-51] and calculated production cross section of ^{52}Mn for proton incidence on ^{nat}Fe. The lines are the same as for Fig.6.

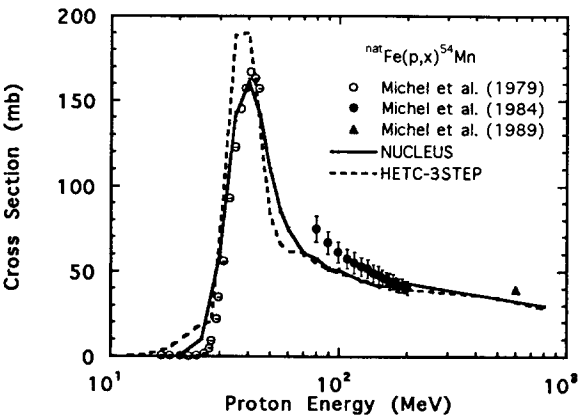

Fig. 28. Experimental[49-51] and calculated production cross section of ^{54}Mn for proton incidence on ^{nat}Fe. The lines are the same as for Fig.6.

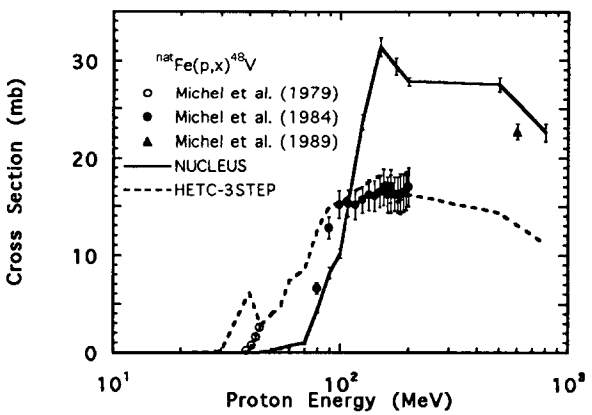

Fig. 29. Experimental[49-51] and calculated production cross section of ^{48}V for proton incidence on ^{nat}Fe. The lines are the same as for Fig.6.

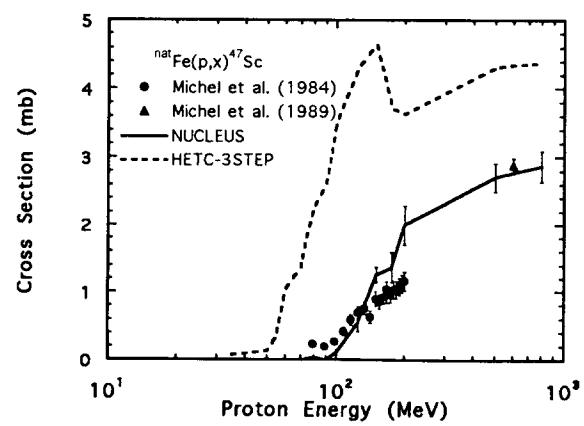

Fig. 30. Experimental[49-51] and calculated production cross section of ^{47}Sc for proton incidence on ^{nat}Fe. The lines are the same as for Fig.6.